

**Matching NLO parton shower matrix element with exact phase space: case of  $W \rightarrow l\nu(\gamma)$  and  $\gamma^* \rightarrow \pi^+\pi^-(\gamma)^\dagger$** **G. Nanava<sup>a</sup>, Qingjun Xu<sup>b</sup> and Z. Was<sup>b,c</sup>**<sup>a</sup> *Physikalisches Institut, Universität Bonn, Nussallee 12, 53115 Bonn, Germany**(On leave from IHEP, TSU, Tbilisi, Georgia)*<sup>b</sup> *Institute of Nuclear Physics, PAN, Kraków, ul. Radzikowskiego 152, Poland*<sup>c</sup> *CERN PH-TH, CH-1211 Geneva 23, Switzerland***ABSTRACT**

In practical applications PHOTOS Monte Carlo is often used for simulation of QED effects in decay of intermediate particles and resonances. Generated in such a way that samples of events cover the whole bremsstrahlung phase space. With the help of selection cuts, experimental acceptance can be then taken into account.

The program is based on exact multiphoton phase space. To evaluate the program precision it is necessary to control its matrix element. Generally it is obtained using iteration of the universal multidimensional kernel. In some cases it is however obtained from the exact first order matrix element. Then, as a consequence, all terms necessary for non-leading logarithms are taken into account. In the present paper we will focus on the decays  $W \rightarrow l\nu$  and  $\gamma^* \rightarrow \pi^+\pi^-$ . The Born level cross sections for both processes approach zero in some points of the phase space.

Process dependent, compensating weight is constructed to implement exact matrix element, but it will be recommended for use only for tests. In the hard photon region, where scalar QED is not expected to be reliable, the compensating weight for  $\gamma^*$  decay can be large. With respect to the total rate, the effect remains at the permille level. It is nonetheless of interest. The terms leading to the effect are analogous to the ones appearing in QCD.

Present paper can be understood either as a contribution to the general discussion on how to match two collinear emission chains resulting from charged sources in a way compatible with the exact and complete phase space and the first order matrix element of QED (scalar QED) or as the practical study of predictions for accelerator experiments.

IFJPAN-IV-2009-1  
CERN-PH-TH/2009-092  
June, 2009

---

<sup>†</sup> This work is partially supported by EU Marie Curie Research Training Network grant under the contract No. MRTN-CT-2006-0355505, Polish Government grant N202 06434 (2008-2010) and EU-RTN Programme: Contract No. MRTN-CT-2006-035482, 'Flavianet'.

# 1 Introduction

One of the crucial aspects of any high energy physics is comparison between results of new measurements and predictions obtained from theory. If agreement is obtained, then the validity domain for the theory is extended. Discrepancy can be attributed to the impact of so called new physics. This scheme is in principle rather simple, but in practice, it is involved. For LEP experiments enormous effort for such program was documented in [1, 2]. It was necessary because for very precise scattering experiments one needs to study radiative corrections simultaneously with detector acceptance. As a consequence, it was possible to confirm experimentally that the Standard Model was indeed a field theory of the elementary particle interactions. Quantum effects could not be omitted, they had to be included in calculations. Importance of this achievement was confirmed by the 1999 year Nobel Prize attributed to 't Hooft and Veltman. Also the last year Nobel Prize for the mechanism of quark flavour mixing [3] required precise measurements and comparison with the data. Such experiments, Belle and BaBar, located respectively in Japan and USA required good control of radiative corrections too [4, 5].

Because of the nature of accelerator experiments, it is generally believed that Monte Carlo technique is the only available tool for the precision comparison of theory and experimental data [1]. Then, effects of detector acceptance can be studied simultaneously with radiative corrections. Multitude of Monte Carlo programs was developed in context of QED [6, 7] and QCD [8, 9], the references can serve as examples.

The basis of such work is always study of expressions obtained by perturbative methods. In the case of QED exponentiation [10] is particularly useful. Exponentiation is now established since long and means rigorous scheme of reorganization of perturbative expansion. It was found [11] that Monte Carlo programs can be developed using such scheme. Significant theoretical effort was nonetheless necessary. It required not only explicit calculation of exact fixed order cross sections, equally important was to separate them into appropriate parts, at the cross section or the spin amplitude level, to finally match results of fixed order calculation with coherent exclusive exponentiation (CEEX) [12] and implement it into computer programs.

QED predicts distributions strongly peaked over the phase space. It may vary by more than 10 orders of magnitude. Complex structure of infrared singularity cancellations, poses a challenge for choice of crude distribution over the phase space too. In the case of multi-photon radiation, particularly elegant method was found. Thanks to conformal symmetry, it was possible to construct crude distribution which was actually exact from the phase space point of view. All simplifications were localized in approximated matrix element. Approximated matrix element consisting of Born amplitude multiplied by the so-called soft factors was used at first. Any further improvements can be easily achieved by correcting weight. The weight is the ratio of distributions calculated from available matrix element obtained perturbatively to given fixed order and the one used in first step of the generation.

The case of QCD is by far more complex, but the general principle is similar. One constructs a simplified matrix element and on its basis (and approximated phase space too) algorithms for the parton showers are build. Such a solution is limited to leading logarithms [13, 14, 15, 16, 17]. Phase space organizations based on so-called orderings are often used [18, 19]. Improvements beyond leading approximations are possible and widely used [20, 21], but have technical diffi-

culties, for example through appearance of negative weight events.

Another major difficulty of QCD is necessity to use parameterization of  $\alpha_s$  at low  $Q^2$  where the standard parameterization  $\alpha_s = \alpha_s(Q^2)$  becomes unreliable<sup>1</sup>. At small scales non-perturbative aspects of QCD can dominate. It leads to further complications and phenomena such as underlying event [24] or hadronization [25]. This of course on top of hadron structure functions obtained from experiments [26].

We will not elaborate in our paper on these topics, however, we think that it may provide useful hint into that direction. First results [27] are encouraging. Our paper is devoted to elaborate on reliability of PHOTOS Monte Carlo. PHOTOS is a Monte Carlo [28, 29] for the QED bremsstrahlung in decays. Its construction is similar to the QED exclusive exponentiation and the parameterization of its phase space generation is exact, but its algorithm is iterative. Conformal symmetry is not used<sup>2</sup>.

As in the cases discussed before, for PHOTOS construction, effort in understanding results of exact perturbative calculations was necessary. It was started from results obtained at the cross section level, Refs. [30, 31] were used. Later, thanks to experience gained in KKMC project [12, 32], spin amplitudes were used as well. In particular, results of Refs. [33, 34, 35] were used. They were essential for design and tests of the program, in particular for choice of the single emission kernels. Thanks to these works, interference of consecutive emissions from charged line as well as interference of emissions from distinct charged lines was properly taken into account, without any need to divide phase space into sectors, each treated differently. That is also why there was no need to separate the photon emission phase space into the regions where either shower or fixed order hard matrix element is used.

Refs. [36, 37, 38] were devoted to numerical tests, but better explanation of the program theoretical foundation was also given there. It may be worth mentioning that for many years the program precision was of no interest and such explanations were delayed nearly to beginning of the present decade. However, it is somehow surprising that this aspect of program development was left unnoticed as late as in 2006 [39].

The best detailed description of the phase space parameterization as used in PHOTOS and explanation that it is actually exact, is given in Refs. [37, 38]. In fact however, it is not different from what was already explained in [28, 29].

The precision of the program is quite amazing. As it was shown in [36, 37], even if incomplete first order matrix element is used in PHOTOS its results agree much better with second order matrix element exclusive exponentiation Monte Carlo KKMC [32] than with KKMC restricted to first order and exponentiation. To quantify the statement, method described in [40, 41] was used. PHOTOS was found to exploit result of perturbative calculation quite well, but it can not be the substitute of such calculations.

The main goal of the present paper is to study spin amplitudes for matching of two parton showers and the hard bremsstrahlung matrix element into interference weight, as in [37, 38]; but now for  $\gamma^* \rightarrow \pi^+\pi^-$  and  $W^\pm \rightarrow l^\pm \nu$ . For that purpose, the matrix element needs to be studied in great detail. Its gauge invariant parts need to be identified and with their help relations with

---

<sup>1</sup> Solutions for this problem were found in [22, 23].

<sup>2</sup>That is why it is similar to solutions used in QCD parton showers, but no phase space ordering of any sort is applied and of course most of the difficulties present in QCD are absent as well.

amplitudes of lower orders have to be found. This second aspect is important and is closely related to properties used in defining factorization schemes, see eg. [42, 43].

Let us point out that in this paper we will not discuss spin amplitudes from the perspective of matching consecutive emissions from the same charged line. Such studies were performed earlier [29], and for other decay. Double emission QED amplitudes are then necessary<sup>3</sup> [35, 34]. We will focus on single photon emission and matching the emissions from two charged lines in case of  $\gamma^* \rightarrow \pi^+\pi^-$ . The analysis of the spin amplitudes and tests for the algorithm in case of Z decay into pair of charged fermion was given earlier, in ref [37]. The case of the scalar particle decay into pair of fermions is covered in [45] and the decay of spinless particle into pair of scalars is studied in [38]. Seemingly, the algorithm works better (correction weights are less important) in the cases where initial state is spinless<sup>4</sup>. The case of W decay was covered in [46], though some approximations were used and decay requires to be revisited.

The two processes are not of the technical interest only, they provide example for studies of Lorentz and gauge group properties of spin amplitudes and cross sections. The  $\gamma^* \rightarrow \pi^+\pi^-$  decay is carefully measured. It is important to improve theoretical uncertainty of PHOTOS for this decay, because of its relevance for establishing  $\alpha_{QED}(M_Z)$  and phenomenology of  $g-2$ . From that perspective, validity of our study is limited by validity of scalar QED<sup>5</sup>. The  $W \rightarrow l\nu$  decay is of interest for precision measurement of W mass and width at LHC for example.

Our paper is organized as follows. In Section 2 we present the scalar QED spin amplitudes for the process  $e^+e^- \rightarrow \gamma^* \rightarrow \pi^+\pi^-(\gamma)$ . It will be shown that the spin amplitudes can be separated into two gauge invariant parts. Section 3 covers further discussion of the amplitudes, and the formulae for cross section used to obtain numerical results. A separation into eikonal part and remaining parts will be presented. Section 4 is devoted to the numerical results obtained with help of MC-TESTER, different option of separating out non-leading effects will be demonstrated. Section 5 is devoted to discussion of further tests, where the beam direction will be used as well. Similarities and differences with respect to the previous case will be underlined. Finally, summary section 6 closes the paper. Spin amplitudes for  $W^\pm \rightarrow l^\pm\nu$  are given in the Appendix.

## 2 Amplitudes

One of the necessary steps in development of any Monte Carlo program is analysis of spin amplitudes. Complete analytical results are often not enough. Usually well known amplitudes have to be revisited again, but this time bearing in mind their structure. It usually manifests factorization properties of the underlying field theory. But it is interesting to check if exact amplitude can be decomposed into sum of gauge invariant parts, which further, can be represented

---

<sup>3</sup>It is probably just to point for inspirations from lectures on QCD [44] but this aspect will still remain waiting for better documentation. Some properties of field theory valid to all orders of perturbation expansion are necessary too. In case of QED it is exponentiation.

<sup>4</sup>This is particularly interesting from the point of view of future attempts to extent into QCD.

<sup>5</sup> This last constraint is of course common with the projects such as PHOKARA [47]. PHOTOS will not be better or worse from that point of view.

as products of gauge invariant terms. Finally, if anything useful can be obtained from such representation.

The spin amplitudes for  $W \rightarrow l\nu\gamma$  are collected in Appendix. In principle they are straightforward and available already in [46] but let us recall them again to clarify possible ambiguities on the way how emission from  $W$  is separated into part of final state radiation and initial state. Let us point to [48], where such issues are discussed. Our expression coincides with the FSR distribution advocated there. This is important point for the discussion of radiative corrections for the purpose of precise measurement of  $W$  lineshape for example. For the case of  $e^+e^- \rightarrow \nu_e \bar{\nu}_e \gamma$  Monte Carlo implementation such discussion can be found in [49].

In the following, let us concentrate on the process  $\gamma^*(p) \rightarrow \pi^+(q_1)\pi^-(q_2)\gamma(k,\epsilon)$ . As precision required by experiments is not that high we will limit ourselves to the case of single photon emission and we will not analyze effects of virtual corrections. At this level it is enough to anticipate their size thanks to Kinoshita-Lee-Nauenberg theorem [50,51]. Anyway, scalar QED predictions for our process are reliable only partly.

The spin structure of our process is new as compared with the previously studied ones like  $Z \rightarrow l^+l^-$ ,  $h \rightarrow l^+l^-$  or  $B^0 \rightarrow \pi^+\pi^-$ . Now the spin of initial state can not be transmitted into helicities of the outgoing particles. That is why we can expect different properties of the amplitudes.

If one considers the process  $e^+e^- \rightarrow \gamma^*(p) \rightarrow \pi^+(q_1)\pi^-(q_2)\gamma(k,\epsilon)$ , the amplitudes equivalent to those given in [52] are obtained. The amplitude can be written as  $M = V^\mu H_\mu$  where  $V_\mu = \bar{v}(p_1, \lambda_1) \gamma_\mu u(p_2, \lambda_2)$ . The  $p_1, \lambda_1, p_2, \lambda_2$  are momenta and helicities of the incoming electron and positron.  $V_\mu$  define the spin state of the intermediate  $\gamma^*$ .

Let us turn now to the part for virtual photon decay. Following conventions of [52], the final interaction part of the Born matrix element for such process is

$$H_0^\mu(p, q_1, q_2) = \frac{eF_{2\pi}(p^2)}{p^2} (q_1 - q_2)^\mu. \quad (1)$$

Here  $p = q_1 + q_2$ . If photon is present, this part of the amplitude reads:

$$H^\mu = \frac{e^2 F_{2\pi}(p^2)}{p^2} \left\{ (q_1 + k - q_2)^\mu \frac{q_1 \cdot \epsilon^*}{q_1 \cdot k} + (q_2 + k - q_1)^\mu \frac{q_2 \cdot \epsilon^*}{q_2 \cdot k} - 2\epsilon^{*\mu} \right\}. \quad (2)$$

This formula can be re-written to the following form:

$$\begin{aligned} H^\mu = & H_0^\mu(p, q_1, q_2) e \left( \frac{q_1 \cdot \epsilon^*}{q_1 \cdot k} - \frac{q_2 \cdot \epsilon^*}{q_2 \cdot k} \right) + \\ & \frac{e^2 F_{2\pi}(p^2)}{p^2} \left( \frac{k^\mu q_1 \cdot \epsilon^* - \epsilon^{*\mu} q_1 \cdot k}{q_1 \cdot k} + \frac{k^\mu q_2 \cdot \epsilon^* - \epsilon^{*\mu} q_2 \cdot k}{q_2 \cdot k} \right). \end{aligned} \quad (3)$$

Formally  $H_0^\mu(p, q_1, q_2)$  is as of the Born case, but instead of  $p = q_1 + q_2$  now  $p = q_1 + q_2 + k$  and such value is used for calculation of virtual photon propagator. Let us note, that the first Born-like term and two other terms in the second line of (3) are separately gauge invariant. Only normalization of space-like part of  $H_0$  is not equal to one of the Born:  $|\vec{q}_1 - \vec{q}_2| < \sqrt{s - 4m_\pi^2}$ . Time-like part of  $H_0$  drops out once product with  $V_\mu$  is taken.

Let us now return to  $V_\mu$ . Following conventions of [53] it reads:

$$V^\mu = 2 \left( |\lambda_+| \hat{e}_1^\mu + i \lambda_+ \hat{e}_2^\mu - m \lambda_- \hat{e}_3^\mu \right). \quad (4)$$

where  $\lambda_\pm = \lambda_1 \pm \lambda_2$ . The vectors satisfy  $(\hat{e}_\alpha)^\mu = \delta_\alpha^\mu$ . We choose  $\hat{e}_1$  to lie in reaction plane, while  $\hat{e}_2 = p_1 \times (q_1 - q_2) / |p_1 \times (q_1 - q_2)|$  is chosen to be perpendicular to that plane. These vectors can be chosen as

$$\hat{e}_0 = \begin{pmatrix} 1 & 0 & 0 & 0 \end{pmatrix}, \hat{e}_1 = \begin{pmatrix} 0 & 1 & 0 & 0 \end{pmatrix}, \hat{e}_2 = \begin{pmatrix} 0 & 0 & 1 & 0 \end{pmatrix}, \hat{e}_3 = \begin{pmatrix} 0 & 0 & 0 & 1 \end{pmatrix}. \quad (5)$$

We can drop the term proportional to electron mass.

At Born level the second term in the expression (4) will not contribute because  $e_2 \cdot (q_1 - q_2) = 0$ . The complete amplitude will read:

$$M_{Born} = e^2 F_{2\pi}(S) \frac{1}{\sqrt{S}} |\lambda_+| \hat{e}_1 \cdot (q_1 - q_2), \quad (6)$$

where  $\sqrt{S}$  is the energy of c.m.. One can see that the amplitude is proportional to  $\sin \theta_B$  as it should be. Here  $\theta_B = \angle p_1 q_1$  is a scattering angle. Squared and summed over initial spin states amplitude gives:

$$\sum_\lambda |M_{Born}|^2(S, T, U) = \frac{8(4\pi\alpha)^2 F_{2\pi}^2(S)}{S^2} (TU - m_\pi^2 S). \quad (7)$$

The Mandelstam variables are defined as follows:

$$S = 2p_1 \cdot p_2, \quad T = 2p_1 \cdot q_1, \quad U = 2p_1 \cdot q_2. \quad (8)$$

Let us now return to amplitudes for single photon emission. Because of the gauge invariance of both parts, it makes sense to rewrite (3) explicitly as sum of two terms:

$$H^\mu = H_I^\mu + H_{II}^\mu \quad (9)$$

or

$$H^\mu = H_{I'}^\mu + H_{II'}^\mu \quad (10)$$

where

$$H_I^\mu = \frac{e^2 F_{2\pi}(p^2)}{p^2} (q_1 - q_2)^\mu \left( \frac{q_1 \cdot \epsilon^*}{q_1 \cdot k} - \frac{q_2 \cdot \epsilon^*}{q_2 \cdot k} \right), \quad (11)$$

$$H_{II}^\mu = \frac{e^2 F_{2\pi}(p^2)}{p^2} \left( k^\mu \left( \frac{q_1 \cdot \epsilon^*}{q_1 \cdot k} + \frac{q_2 \cdot \epsilon^*}{q_2 \cdot k} \right) - 2\epsilon^{*\mu} \right), \quad (12)$$

and alternatively

$$H_{I'}^\mu = \frac{e^2 F_{2\pi}(p^2)}{p^2} \left( (q_1 - q_2)^\mu + k^\mu \frac{q_2 \cdot k - q_1 \cdot k}{q_2 \cdot k + q_1 \cdot k} \right) \left( \frac{q_1 \cdot \epsilon^*}{q_1 \cdot k} - \frac{q_2 \cdot \epsilon^*}{q_2 \cdot k} \right), \quad (13)$$

$$H_{II'}^\mu = \frac{2e^2 F_{2\pi}(p^2)}{p^2} \left( \frac{k^\mu}{q_2 \cdot k + q_1 \cdot k} (q_1 \cdot \epsilon^* + q_2 \cdot \epsilon^*) - \epsilon^{*\mu} \right). \quad (14)$$

### 3 Cross section and separation of amplitude into parts

Before going into numerical results, let us elaborate on the formulas presented above in more details. One can see rather easily, that formulas (11) and (13) have a form typical for amplitudes of QED exclusive exponentiation [54], that is Born factor multiplied by eikonal factor  $\left(\frac{q_1 \cdot \epsilon^*}{q_1 \cdot k} - \frac{q_2 \cdot \epsilon^*}{q_2 \cdot k}\right)$ . In fact, the two expressions differ in the way how the Born factor differs from the genuine Born expression. In both cases expressions indeed approach the Born one in soft photon limit, but in case of (13) this property holds also in case when photon is collinear to  $\pi^+$  or  $\pi^-$ . This was achieved by adding to (13) the term proportional to  $k^\mu \frac{q_2 \cdot k - q_1 \cdot k}{q_2 \cdot k + q_1 \cdot k}$  and subtracting it from (14). As a consequence the expression in first bracket of (13), in collinear configurations will be close to  $q_1 - q_2 \mp k$  respectively if  $q_1 \cdot k \ll q_2 \cdot k$  and  $q_2 \cdot k \ll q_1 \cdot k$ . Thus, it is consistent with LL level factorization into Born amplitude and eikonal factor. In general case expressions (11) and (13) differ from product of Born times eikonal factor only by normalization. This defect is easy to correct numerically and we will return to this point later in this section when discussion of cross section will be given.

Experience with the  $Z \rightarrow l^+ l^-$  decay has shown that it is useful not only to rely on spin amplitudes, but to collect expressions for amplitudes squared and (partly) averaged over the spin degrees of freedom. That can be useful in case of future work on matching kernels for consecutive emissions.

If one takes separation (9) for the calculation of two parts of spin amplitudes, after spin average, the expression for the cross section takes the form:

$$\sum_{\lambda, \epsilon} |M|^2 = \sum_{\lambda, \epsilon} |M_I|^2 + \sum_{\lambda, \epsilon} |M_{II}|^2 + 2 \sum_{\lambda, \epsilon} M_I M_{II}^*, \quad (15)$$

where

$$\begin{aligned} \sum_{\lambda, \epsilon} |M_I|^2 &= -2e^6 \frac{F_{2\pi}^2(S)}{S^2} \left( \frac{m_\pi^2}{(q_1 \cdot k)^2} + \frac{m_\pi^2}{(q_2 \cdot k)^2} - \frac{S'}{(q_1 \cdot k)(q_2 \cdot k)} \right) \\ &\quad \{ (TU' - m_\pi^2 S) + (T'U - m_\pi^2 S) - (TT' + UU' - SS') \} \\ &= -(\pi\alpha) \left( \frac{m_\pi^2}{(q_1 \cdot k)^2} + \frac{m_\pi^2}{(q_2 \cdot k)^2} - \frac{S'}{(q_1 \cdot k)(q_2 \cdot k)} \right) (A + B + C + D) + \\ &\quad 8e^6 \frac{F_{2\pi}^2(S)}{S^2} \left( \frac{m_\pi^2}{(q_1 \cdot k)^2} + \frac{m_\pi^2}{(q_2 \cdot k)^2} - \frac{S'}{(q_1 \cdot k)(q_2 \cdot k)} \right) (q_1 \cdot k)(q_2 \cdot k), \quad (16) \end{aligned}$$

$$\begin{aligned}
\sum_{\lambda, \varepsilon} |M_{II}|^2 &= -2e^6 \frac{F_{2\pi}^2(S)}{S^2} \left\{ \left( \frac{m_\pi^2}{(q_1 \cdot k)^2} + \frac{m_\pi^2}{(q_2 \cdot k)^2} + \frac{S'}{(q_1 \cdot k)(q_2 \cdot k)} \right) \right. \\
&\quad \left( (TU' - m_\pi^2 S) + (T'U - m_\pi^2 S) + (TT' + UU' - SS') \right) - 8S \\
&\quad + \frac{4}{q_1 \cdot k} \left( TU' - m_\pi^2 S + \frac{1}{2}(TT' + UU' - SS') \right) \\
&\quad \left. + \frac{4}{q_2 \cdot k} \left( T'U - m_\pi^2 S + \frac{1}{2}(TT' + UU' - SS') \right) \right\} \\
&= -(\pi\alpha) \frac{F_{2\pi}^2(S)}{S^2} \left\{ \left( \frac{m_\pi^2}{(q_1 \cdot k)^2} + \frac{m_\pi^2}{(q_2 \cdot k)^2} + \frac{S'}{(q_1 \cdot k)(q_2 \cdot k)} \right) \right. \\
&\quad \left( A + B - C - D \right) + \frac{4}{q_1 \cdot k} \left( B - \frac{1}{2}(C + D) \right) + \frac{4}{q_2 \cdot k} \left( A - \frac{1}{2}(C + D) \right) \Big\} \\
&\quad - 8e^6 \frac{F_{2\pi}^2(S)}{S^2} \left( \frac{m_\pi^2}{(q_1 \cdot k)^2} + \frac{m_\pi^2}{(q_2 \cdot k)^2} + \frac{S'}{(q_1 \cdot k)(q_2 \cdot k)} \right) (q_1 \cdot k)(q_2 \cdot k) \\
&\quad + 8e^6 \frac{F_{2\pi}^2(S)}{S^2} (S' + 2m_\pi^2 + S), \tag{17}
\end{aligned}$$

$$\begin{aligned}
2 \sum_{\lambda, \varepsilon} M_I M_{II}^* &= -4e^6 \frac{F_{2\pi}^2(S)}{S^2} \left\{ \left( \frac{m_\pi^2}{(q_1 \cdot k)^2} - \frac{m_\pi^2}{(q_2 \cdot k)^2} \right) \right. \\
&\quad \left( - (TU' - m_\pi^2 S) + (T'U - m_\pi^2 S) \right) \\
&\quad - \frac{2}{q_1 \cdot k} \left( TU' - m_\pi^2 S - \frac{1}{2}(TT' + UU' - SS') \right) \\
&\quad \left. + \frac{2}{q_2 \cdot k} \left( - (T'U - m_\pi^2 S) + \frac{1}{2}(TT' + UU' - SS') \right) \right\} \\
&= -(\pi\alpha) \left\{ \left( \frac{m_\pi^2}{(q_1 \cdot k)^2} - \frac{m_\pi^2}{(q_2 \cdot k)^2} \right) (2A - 2B) - \frac{4}{q_1 \cdot k} \left( B + \frac{1}{2}(C + D) \right) \right. \\
&\quad \left. - \frac{4}{q_2 \cdot k} \left( A + \frac{1}{2}(C + D) \right) \right\} + 8e^6 \frac{F_{2\pi}^2(S)}{S^2} (S' + 2m_\pi^2 - S). \tag{18}
\end{aligned}$$

The definitions of terms like  $A, B, C, D, E$  will be given later in the section.

If instead of expression (9) we use (10) the following expressions are obtained:

$$\sum_{\lambda, \varepsilon} |M|^2 = \sum_{\lambda, \varepsilon} |M_{I'}|^2 + \sum_{\lambda, \varepsilon} |M_{II'}|^2 + 2 \sum_{\lambda, \varepsilon} M_{I'} M_{II'}^*, \tag{19}$$



where

$$\begin{aligned}
\sum_{\lambda, \epsilon} |M_{I'}|^2 &= -8e^6 \frac{F_{2\pi}^2(S)}{S^2} \left( \frac{m_\pi^2}{(q_1 \cdot k)^2} + \frac{m_\pi^2}{(q_2 \cdot k)^2} - \frac{S'}{(q_1 \cdot k)(q_2 \cdot k)} \right) \\
&\quad \left\{ \frac{(q_1 \cdot k)^2}{(q_1 \cdot k + q_2 \cdot k)^2} (TU' - m_\pi^2 S) + \frac{(q_2 \cdot k)^2}{(q_1 \cdot k + q_2 \cdot k)^2} (T'U - m_\pi^2 S) - \right. \\
&\quad \left. \frac{(q_1 \cdot k)(q_2 \cdot k)}{(q_1 \cdot k + q_2 \cdot k)^2} (TT' + UU' - SS') \right\} \\
&= -(4\pi\alpha) \left( \frac{m_\pi^2}{(q_1 \cdot k)^2} + \frac{m_\pi^2}{(q_2 \cdot k)^2} - \frac{S'}{(q_1 \cdot k)(q_2 \cdot k)} \right) \\
&\quad \left( \frac{(q_2 \cdot k)^2}{(q_1 \cdot k + q_2 \cdot k)^2} A + \frac{(q_1 \cdot k)^2}{(q_1 \cdot k + q_2 \cdot k)^2} B + \frac{(q_1 \cdot k)(q_2 \cdot k)}{(q_1 \cdot k + q_2 \cdot k)^2} (C + D) \right) + \\
&\quad 32e^6 \frac{F_{2\pi}^2(S)}{S^2} \left( \frac{m_\pi^2}{(q_1 \cdot k)^2} + \frac{m_\pi^2}{(q_2 \cdot k)^2} - \frac{S'}{(q_1 \cdot k)(q_2 \cdot k)} \right) \frac{(q_1 \cdot k)^2 (q_2 \cdot k)^2}{(q_1 \cdot k + q_2 \cdot k)^2}, \quad (20)
\end{aligned}$$

$$\begin{aligned}
\sum_{\lambda, \epsilon} |M_{II'}|^2 &= \frac{-8e^6 F_{2\pi}^2(S)}{S^2} \left[ \frac{S}{(q_1 \cdot k + q_2 \cdot k)^2} (TU' - m_\pi^2 S + T'U - m_\pi^2 S + TT' + UU' - SS') \right. \\
&\quad \left. - 2S \right] \\
&= \frac{-(4\pi\alpha)S}{(q_1 \cdot k + q_2 \cdot k)^2} (A + B - C - D) + \frac{16e^6 F_{2\pi}^2(S)}{S^2} \frac{(q_1 \cdot k)^2 + (q_2 \cdot k)^2}{(q_1 \cdot k + q_2 \cdot k)^2} S. \quad (21)
\end{aligned}$$

Note that this part is free of infrared and collinear divergences.

$$\begin{aligned}
2 \sum_{\lambda, \epsilon} M_{I'} M_{II'}^* &= \frac{-8e^6 F_{2\pi}^2(S)}{S^2} \frac{1}{(q_1 \cdot k + q_2 \cdot k)^2} \left\{ \left( (2m_\pi^2 + S') \frac{q_1 \cdot k}{q_2 \cdot k} - S \right) (TU' - m_\pi^2 S) + \right. \\
&\quad \left( (2m_\pi^2 + S') \frac{q_2 \cdot k}{q_1 \cdot k} - S \right) (T'U - m_\pi^2 S) + \\
&\quad \left( \frac{S}{2} \left( \frac{q_1 \cdot k}{q_2 \cdot k} + \frac{q_2 \cdot k}{q_1 \cdot k} \right) - 2m_\pi^2 - S' \right) (TT' + UU' - SS') \right\} \\
&= \frac{-4\pi\alpha}{(q_1 \cdot k + q_2 \cdot k)^2} \left\{ \left( (2m_\pi^2 + S') \frac{q_2 \cdot k}{q_1 \cdot k} - S \right) A + \left( (2m_\pi^2 + S') \frac{q_1 \cdot k}{q_2 \cdot k} - S \right) B \right. \\
&\quad \left. - \left( \frac{S}{2} \left( \frac{q_1 \cdot k}{q_2 \cdot k} + \frac{q_2 \cdot k}{q_1 \cdot k} \right) - 2m_\pi^2 - S' \right) (C + D) \right\} - \\
&\quad \frac{32e^6 F_{2\pi}^2(S)}{S^2 (q_1 \cdot k + q_2 \cdot k)^2} \left[ \frac{S}{2} ((q_1 \cdot k)^2 + (q_2 \cdot k)^2) - (2m_\pi^2 + S')(q_1 \cdot k)(q_2 \cdot k) \right]. \quad (22)
\end{aligned}$$

The definition of Mandelstam variables is

$$S = 2p_1 \cdot p_2, \quad S' = 2q_1 \cdot q_2, \quad (23)$$

$$T = 2p_1 \cdot q_1, \quad T' = 2p_2 \cdot q_2, \quad (24)$$

$$U = 2p_1 \cdot q_2, \quad U' = 2p_2 \cdot q_1. \quad (25)$$

For later convenience, we define

$$A = \sum_{\lambda} |M_{Born}|^2(S, T', U), \quad (26)$$

$$B = \sum_{\lambda} |M_{Born}|^2(S, T, U'), \quad (27)$$

$$C = \sum_{\lambda} |M_{Born}|^2(S, T, U), \quad (28)$$

$$D = \sum_{\lambda} |M_{Born}|^2(S, T', U'), \quad (29)$$

$$E = 32(4\pi\alpha)^3 m_\pi^2 \frac{F_{2\pi}^2(S)}{S^2}. \quad (30)$$

Finally let us point out, that complete expression for the amplitude squared can be given in the following elegant form:

$$\sum_{\lambda, \varepsilon} |M|^2 = 4\pi\alpha \left\{ \frac{-m_\pi^2}{(q_1 \cdot k)^2} A + \frac{-m_\pi^2}{(q_2 \cdot k)^2} B + \frac{S - 2m_\pi^2}{2(q_1 \cdot k)(q_2 \cdot k)} (C + D) \right\} + E. \quad (31)$$

We should stress that above two separation options (15) and (19) can have their first terms even closer to Born-times-eikonal-factor form. For that purpose it is enough to adjust normalization of (11) (or (13)) to Born amplitude times eikonal factor. Compensating adjustment to (12) (or (14)) is then necessary. The changes can be performed by numerical manipulation of the three contributions to (15) and (19). The resulting new separation into parts will be distinguished by additional prime over its parts. For example  $\sum_{\lambda, \varepsilon} |M'_{II}|^2$  will be used instead of  $\sum_{\lambda, \varepsilon} |M_{II}|^2$ .

Such a modification is of interest, because if  $\sum_{\lambda, \varepsilon} |M'_I|^2$  or  $\sum_{\lambda, \varepsilon} |M'_{II}|^2$  is used alone, then it is the expression used in PHOTOS Monte Carlo with refinement of [38]. In the next section, we will perform our numerical investigations with respect to [38] which is for us an approximation only.

## 4 General numerical results

We have performed our studies at virtualities for the decaying photon of 2, 20, 200 and 2000 GeV. However in the paper we will show only the case of 2 GeV. The other ones confirm only that the collinear logarithms are properly reproduced by the simulation with standard set-up of PHOTOS kernel and would bring nothing to our discussion, targeting effect going beyond that level.

Let us start with presentation of the case when weight for the matrix element is that for  $\sum_{\lambda,\epsilon} |M'_I|^2$  or  $\sum_{\lambda,\epsilon} |M'_{I'}|^2$ . As one can see from fig.1 agreement with matrix element of [38] is excellent all over the phase space. Unfortunately as it will be discussed in the next section this is true only for the case when distributions are averaged over the orientation of the whole event with respect to incoming beams (or spin state of the virtual photon). At this moment let us point that as a consequence of strongly varying Born cross section (approaching zero in forward and backward direction) the resulting weight from  $\sum_{\lambda,\epsilon} |M'_I|^2$  or  $\sum_{\lambda,\epsilon} |M'_{I'}|^2$  has a tail. We have used special techniques to appropriately adopt Monte Carlo simulation for that.

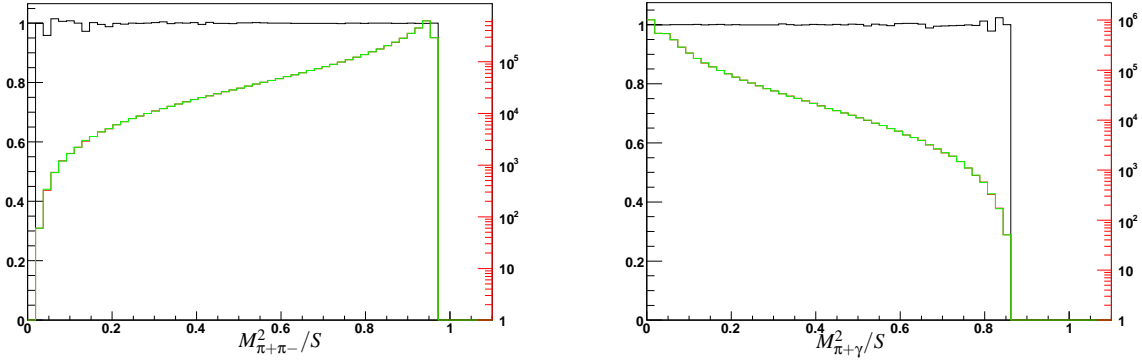
If instead of  $\sum_{\lambda,\epsilon} |M'_I|^2$  or  $\sum_{\lambda,\epsilon} |M'_{I'}|^2$  one would use directly  $\sum_{\lambda,\epsilon} |M_I|^2$  or  $\sum_{\lambda,\epsilon} |M_{I'}|^2$ , that is when normalization of Born-like factor is not performed, differences with respect to formulas of [38] are much larger, see respectively figs 2 and 3. In the last case discrepancies are smaller, because normalization is correct for collinear configurations. Finally let us compare results of complete scalar QED matrix element with that of [38], see fig. 4. At high photon energy region there is clear surplus of events with respect to formulas of [38]. That contribution should not be understood as bremsstrahlung, but rather as genuine process. Anyway in that region of phase space scalar QED is not expected to work well. Even though expression (31) looks elegant and is short, it needs to be separated into (at the cross section level) longer ones, because those make sense when they are confronted with Born times eikonal factor expression. We cannot conclude that at this point we understand all properties of amplitude parts. Note however that the difference between results of figs 1 and 4 constitutes only 0.2 % of the total process rate. That is why our detailed discussion is not important for numerical conclusions, but for the understanding of the underlying structure. On the other hand, once status of approximation used in PHOTOS at single photon radiation is established, we can use it to calculate effects of higher orders simultaneously with the detector effects. As example we show comparison of single photon emission PHOTOS, with the run where multiple emission is activated, see fig.5. Effects are rather small. This could be not the case if selection cuts would be present.

Now, let us consider the decay  $W \rightarrow l\nu(\gamma)$ . In [46] simple correcting weight was introduced into PHOTOS to correct discrepancies with respect to exact predictions of SANC [55] Monte Carlo for this decay. At present weight based on the exact matrix element, see Appendix, is available. So one can check again how good this approximation was. As one can see from fig. 6 the correction weight reproduces well result of exact matrix element. In fig. 7 we show that once exact matrix element is implemented into PHOTOS agreement with the benchmark calculation is better than statistical error of  $10^8$  events. In contrary to the previously studied  $\gamma^* \rightarrow \pi^+\pi^-\gamma$  case, there were no problems with the weight tail.

## 5 Numerical results using beam direction

In the previous section we have discussed distributions build out of four momenta of decay products only. Agreement between results of PHOTOS using universal kernel and simulations based on matrix element was excellent both in case of  $W \rightarrow l\nu(\gamma)$  and  $\gamma^* \rightarrow \pi^+\pi^-(\gamma)$  decays, even

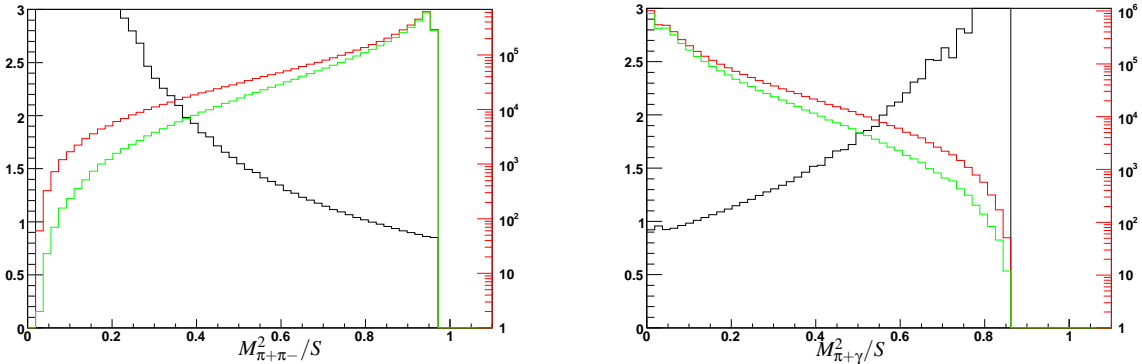
Figure 1: Distributions of invariant masses normalized to center of mass energy and squared ( $M^2/S$ ) for  $e^+e^- \rightarrow \pi^+\pi^-(\gamma)$  at 2 GeV center of mass energy. Results from PHOTOS with matrix element taken from [38] are given in red colour. If matrix element  $\sum_{\lambda,\epsilon} |M'_I|^2$  or  $\sum_{\lambda,\epsilon} |M'_{I'}|^2$  is used (the two options are effectively identical) results are given in green colour. Logarithmic scale is used, but for the ratio (black line) linear scale is used instead. Fraction of events with photons above 50 MeV is respectively  $4.2279 \pm 0.0021$  % and  $4.2269 \pm 0.0021$  % for the two programs.



(a) This distribution is identical to the distribution of photon energy in the reaction frame as well.

(b) This distribution coincides with distributions for invariant mass of  $\pi^-\gamma$  pair.

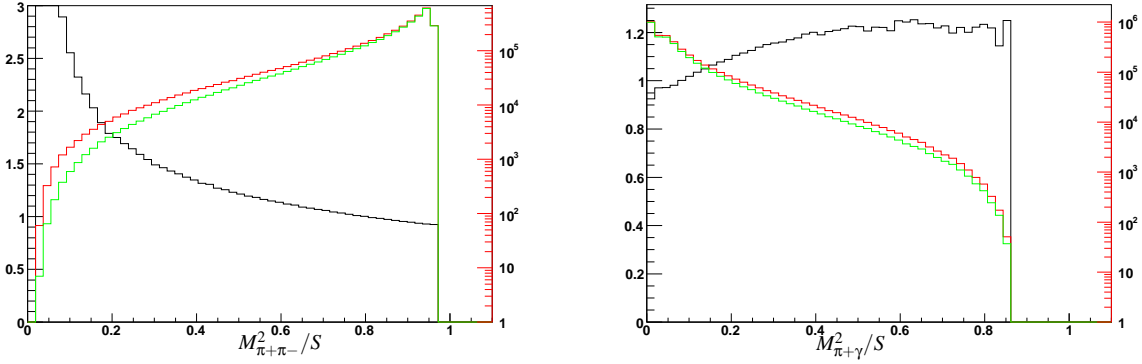
Figure 2: Distributions of invariant masses normalized to center of mass energy and squared ( $M^2/S$ ) for  $e^+e^- \rightarrow \pi^+\pi^-(\gamma)$  at 2 GeV center of mass energy. Results from PHOTOS with matrix element taken from [38] are given in red colour. If matrix element  $|M_I|^2$  is used results are given in green colour. Logarithmic scale is used, but for the ratio (black line) linear scale is used instead. Fraction of events with photons above 50 MeV is respectively  $4.2279 \pm 0.0021$  % and  $3.4435 \pm 0.0019$  % for the two programs.



(a) This distribution is identical to the distribution of photon energy in the reaction frame as well.

(b) It coincides with distributions for invariant mass of  $\pi^-\gamma$  pair.

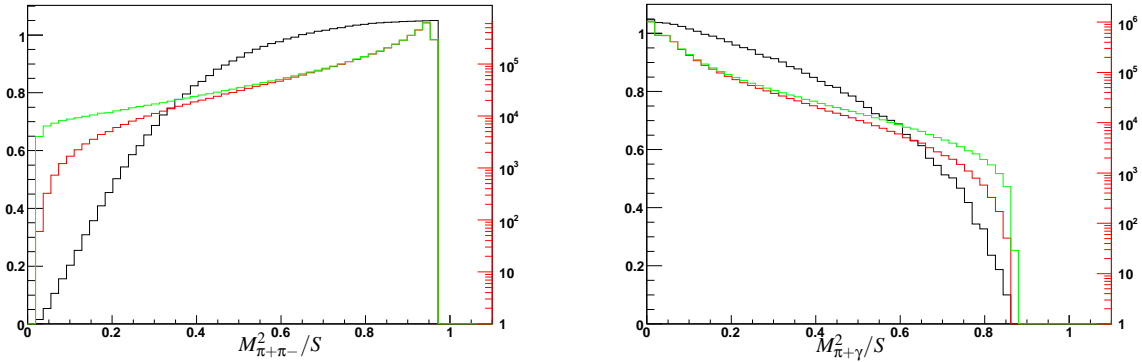
Figure 3: Distributions of invariant masses normalized to center of mass energy and squared ( $M^2/S$ ) for  $e^+e^- \rightarrow \pi^+\pi^-(\gamma)$  at 2 GeV center of mass energy. Results from PHOTOS with matrix element taken from [38] are given in red colour. If matrix element  $\sum_{\lambda,\epsilon} |M_{\gamma}|^2$  is used results are given in green colour. Logarithmic scale is used, but for the ratio (black line) linear scale is used instead. Fraction of events with photons above 50 MeV is respectively  $4.2279 \pm 0.0021$  % and  $3.8329 \pm 0.0020$  % for the two programs.



(a) This distribution is identical to the distribution of photon energy in the reaction frame as well.

(b) It coincides with distributions for invariant mass of  $\pi^-\gamma$  pair.

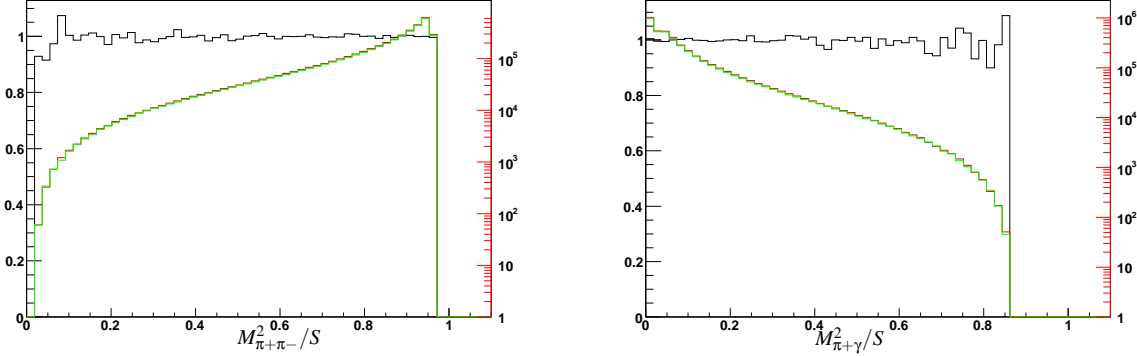
Figure 4: Distributions of invariant masses normalized to center of mass energy and squared ( $M^2/S$ ) for  $e^+e^- \rightarrow \pi^+\pi^-(\gamma)$  at 2 GeV center of mass energy. Results from PHOTOS with matrix element taken from [38] are given in red colour. If complete matrix element is used results are given in green colour. Logarithmic scale is used, but for the ratio (black line) linear scale is used instead. Fraction of events with photons above 50 MeV is respectively  $4.2279 \pm 0.0021$  % and  $4.4320 \pm 0.0021$  % for the two programs.



(a) This distribution is identical to the distribution of photon energy in the reaction frame as well.

(b) It coincides with distributions for invariant mass of  $\pi^-\gamma$  pair.

Figure 5: Distributions of invariant masses normalized to center of mass energy and squared ( $M^2/S$ ) for  $e^+e^- \rightarrow \pi^+\pi^-(\gamma)$  at 2 GeV center of mass energy. Results from PHOTOS with matrix element taken from [38] are given in red colour. If exponentiation option is activated and matrix element of [38] is used again results are given in green colour. Logarithmic scale is used, but for the ratio (black line) linear scale is used instead. Fraction of events with at least one photon above 50 MeV is respectively  $4.2279 \pm 0.0021 \%$  and  $4.1377 \pm 0.0020\%$  for the two programs.



(a) This distribution is identical to the distribution of photon energy in the reaction frame as well.

(b) It coincides with distributions for invariant mass of  $\pi^-\gamma$  pair.

though in the PHOTOS kernel effects of the decaying particle spin was not taken into account<sup>6</sup>.

As can be seen from the plots 8–11, distributions where orientation of the  $W$  boson spin matters are getting affected. The plots 8 and 9 show the photon momentum distributions with respect to a spin quantization axis as predicted by SANC and by PHOTOS with the standard kernel in transversally and longitudinally polarized  $W$  boson decays. The plots 10 and 11 correspond to the muon momentum distributions. The regions of phase space where distributions are sparsely populated and where in fact at Born level probability density approaches zero are becoming moderately overpopulated by PHOTOS (increase of up to 14 % of density was found for transversely polarized  $W$  boson decay). This is probably, in most cases, of no practical consequences, nonetheless requires quantification. Once exact matrix element is implemented into PHOTOS agreement with the SANC predictions is better than statistical error of  $10^8$  events, see fig. 12.

Similar effect takes place for  $\gamma^* \rightarrow \pi^+\pi^-\gamma$ . Even though from fig. 1 one could conclude that the universal kernel of [38], for arbitrary large samples, is equivalent to the matrix element as given by  $\sum_{\lambda,\epsilon} |M'_I|^2$  or  $\sum_{\lambda,\epsilon} |M'_{I'}|^2$ , differences appear in distributions sensitive to initial state spin orientation, see figs 13 and 14. On these plots angular distributions of the photon momentum with respect to the beam line are shown. Again, regions of phase space giving zero contribution at the Born level are becoming overpopulated if approximation for the photon radiation matrix element is used. From that perspective and for practical reasons one can conclude that the

<sup>6</sup>This is definitely a complication requiring some attention. It is interesting aspect of PHOTOS validation, absent in case of the scalar state [38], but present in case of  $Z$  decay [37], and it is strongly related to limits of factorization.

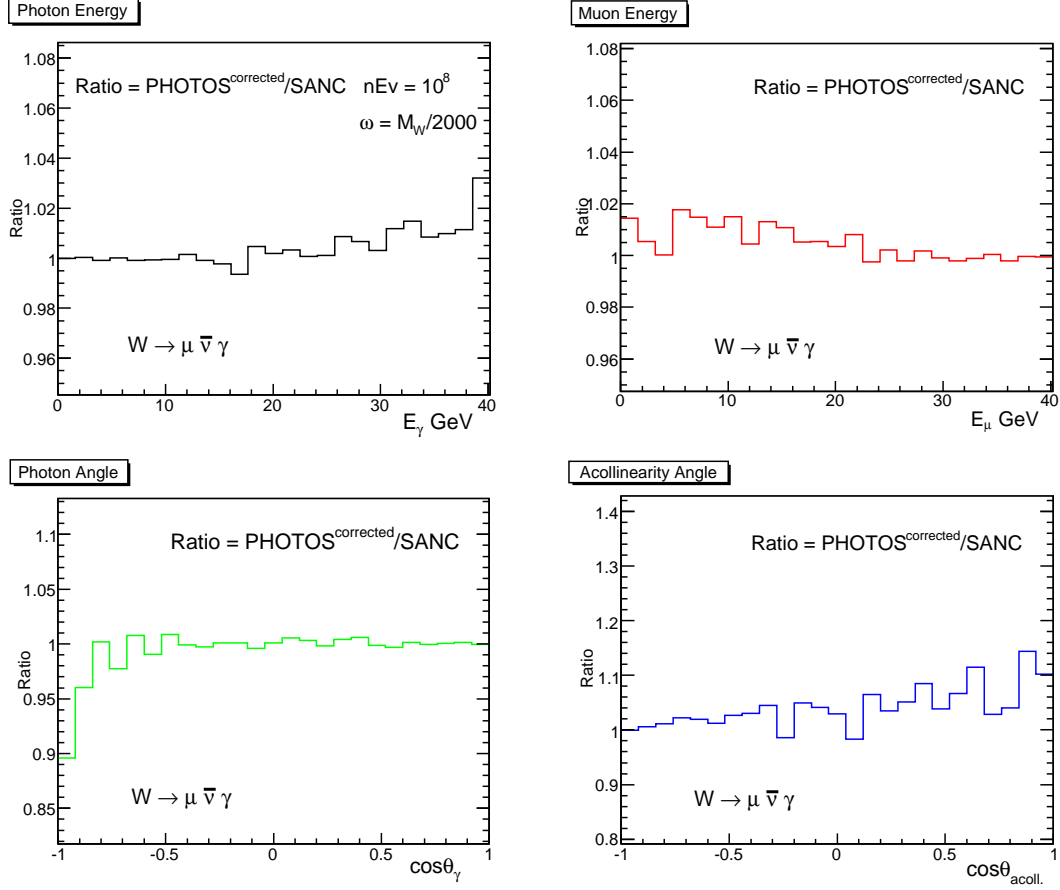


Figure 6: Ratios of the results from PHOTOS with correcting weight and SANC for the  $W \rightarrow l\bar{\nu}(\gamma)$  decay distributions are shown.

$\sum_{\lambda,\varepsilon} |M'_{I'}|^2$  choice is better than  $\sum_{\lambda,\varepsilon} |M'_I|^2$ . It gives distributions closer to the ones obtained from universal kernel. The remaining part of (19) represents better corrections for complete matrix element necessary for the results obtained with universally set PHOTOS. We can see also that distributions obtained from kernel of ref. [38] and  $\sum_{\lambda,\varepsilon} |M'_I|^2$  are only close to each other but nonetheless distinct. The zero of Born level decay distribution for  $\gamma^*$  in angle  $\cos\theta_{\pi^\pm} = \pm 1$  is of more practical consequences than zero in Born level  $W$  decay distribution. Internal weight of PHOTOS for exact matrix element becomes large in well defined corners of the phase space of  $\gamma^*$  decay, see fig. 4.

## 6 Summary

In the present paper we have studied matrix elements for the processes  $\gamma^* \rightarrow \pi^+\pi^-\gamma$  and  $W \rightarrow l\nu\gamma$ . We could observe that the expressions separate into gauge invariant parts. In both  $W \rightarrow l\nu$  and  $\gamma^* \rightarrow \pi^+\pi^-\gamma$  cases, part consisting of eikonal factor multiplying spin amplitude of the Born level is separated. It is the part which contributes to infrared singularity. In case of  $\gamma^* \rightarrow$

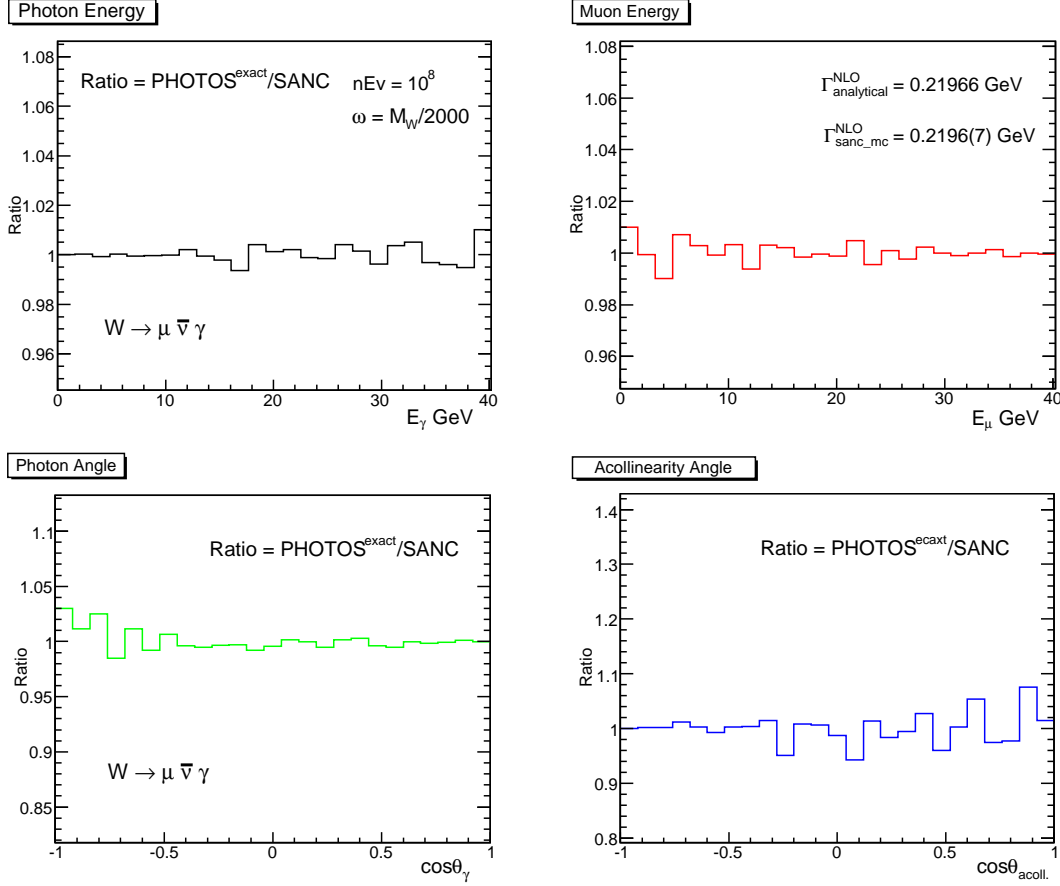


Figure 7: Ratios of the results from PHOTOS with correcting weight and SANC for the  $W \rightarrow l\bar{\nu}(\gamma)$  decay distributions are shown.

$\pi^+\pi^-\gamma$  the remaining part does not contribute to collinear singularity but for  $W \rightarrow l\nu$  it can be separated further: into part proportional to  $W$  charge which does not lead after integration to any logarithmic contribution, and the part proportional to lepton charge which contribute to collinear singularity but is identical to analogous part for the process  $Z \rightarrow l^+l^-$  (see eg. second or third part of formula 5 in [27]). That is exactly the factorization property needed for the iterative solution used in PHOTOS to be valid for multiphoton emissions and processes discussed in present paper.

For  $\gamma^* \rightarrow \pi^+\pi^-\gamma$ , the factor, identified as Born level amplitude, is not unique. Ambiguity is, as expected, proportional to photon momentum, it disappears in soft limit. Resulting from the ambiguity options were identified. This is of no practical consequences for the present work, but should be kept in mind if the obtained spin amplitude parts would be used as building brick for amplitudes of more elaborated processes.

We have identified dominant parts of spin amplitudes and used them for tests and for kernels of PHOTOS Monte Carlo. Exact matrix element was used for that purpose too. We have found, that whole matrix element for the process  $W \rightarrow l\nu\gamma$  can be incorporated into photon emission kernel. On the other hand for  $\gamma^* \rightarrow \pi^+\pi^-\gamma$  it is not straightforward, because of occurrence of



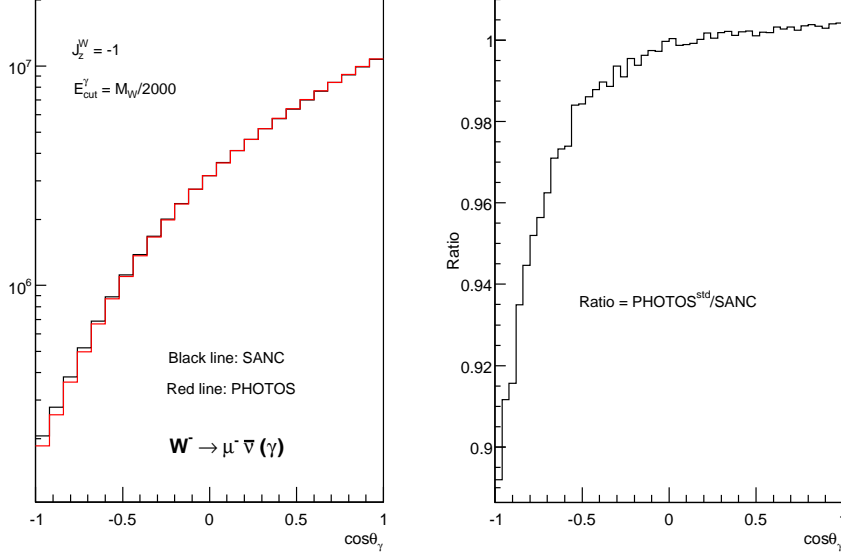


Figure 8: Cosine of the photon momentum with respect to spin axis in the decay  $W \rightarrow l\bar{\nu}(\gamma)$  is shown.  $W$  boson is transversely polarized,  $J_z^W = -1$ , with respect this axis. The black line corresponds to SANC results, while the red line corresponds to predictions of PHOTOS with standard kernel.

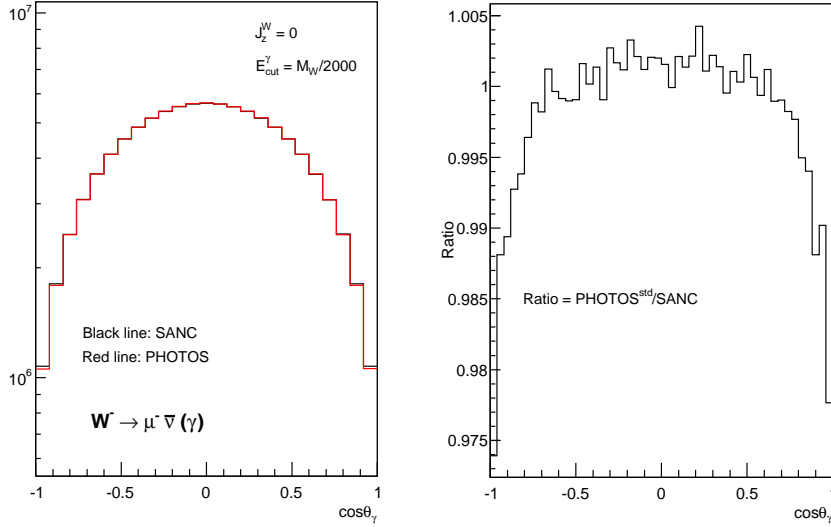


Figure 9: Cosine of the photon momentum with respect to spin axis in the decay  $W \rightarrow l\bar{\nu}(\gamma)$  is shown.  $W$  boson is longitudinally polarized,  $J_z^W = 0$ . The black line corresponds to SANC results, while the red line corresponds to predictions of PHOTOS with standard kernel.

large weight events. The responsible term was identified and it may be interesting to point that it is similar to the one obtained in different calculation ([27] formula (68)). There, such terms were interpreted as contributing to running of QCD coupling constant. In fact the term involves

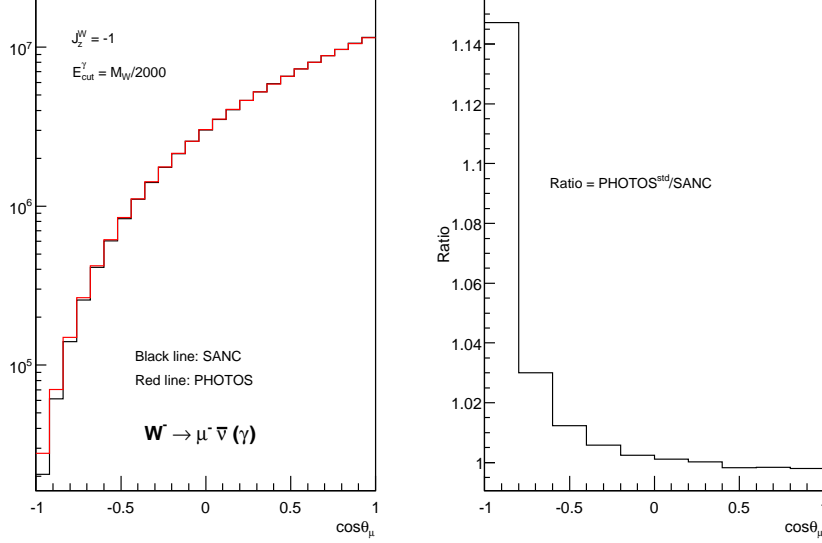


Figure 10: Cosine of the muon momentum with respect to spin axis in the decay  $W \rightarrow l\bar{\nu}(\gamma)$  is shown.  $W$  boson is transversally polarized,  $J_z^W = -1$ . The black line corresponds to SANC results, while the red line corresponds to predictions of PHOTOS with standard kernel. Lack of spin effects in PHOTOS standard kernel results in up to 14% surplus of events in regions approaching zero for the distribution as predicted from Born level.

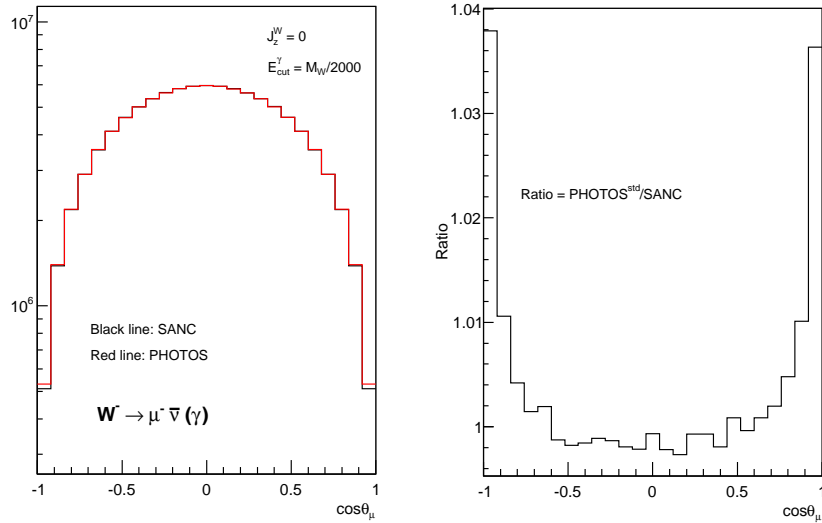


Figure 11: Cosine of the muon momentum with respect to spin axis in the decay  $W \rightarrow l\bar{\nu}(\gamma)$  is shown.  $W$  boson is longitudinally polarized,  $J_z^W = 0$ . The black line corresponds to SANC results, while the red line corresponds to predictions of PHOTOS with standard kernel. Lack of spin effects in PHOTOS standard kernel results in up to 4% surplus of events in regions approaching zero for the distribution as predicted from Born level.

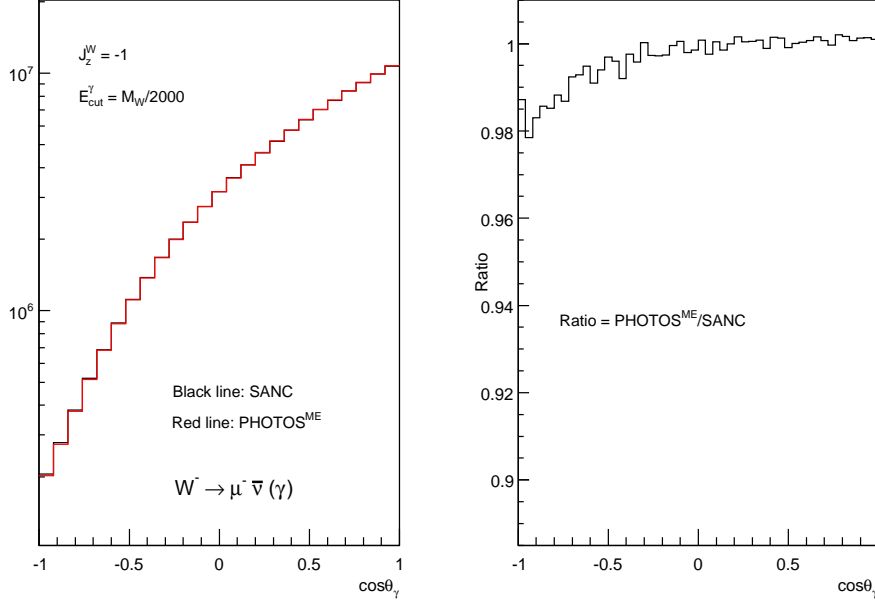
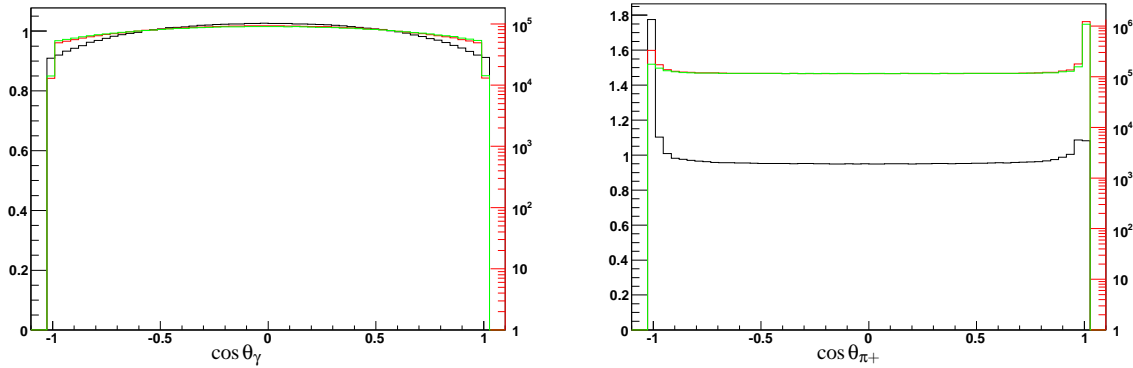


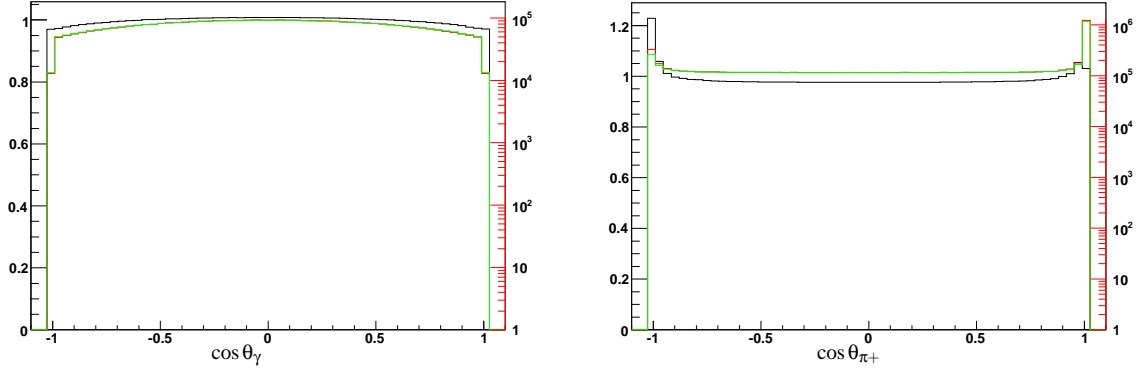
Figure 12: Cosine of the photon momentum with respect to spin axis in the decay  $W \rightarrow l\bar{\nu}(\gamma)$  is shown.  $W$  boson is transversely polarized,  $J_z^W = -1$ , along this axis. The black line corresponds to SANC results, while the red line corresponds to predictions of PHOTOS with exact matrix element.

Figure 13: Angular distributions for  $e^+e^- \rightarrow \pi^+\pi^-(\gamma)$  at 2 GeV center of mass energy. Results from PHOTOS with matrix element taken from [38] are given in red colour. Matrix element  $\sum_{\lambda,\epsilon} |M'_I|^2$  is used for results with green line. Logarithmic scale is used, but for the ratio (black line) linear scale is used instead. Fraction of presented events (i.e. with photons above 50 MeV) is respectively  $4.2279 \pm 0.0021\%$  and  $4.2269 \pm 0.0021\%$  of the total samples for the two programs.



(a) cosine of the photon angle with respect to beam is shown. (b) cosine of the  $\pi^+$  angle with respect to the same charge beam is shown.

Figure 14: Angular distributions for  $e^+e^- \rightarrow \pi^+\pi^-\gamma$  at 2 GeV center of mass energy. Results from PHOTOS with matrix element taken from [38] are given in red colour.  $\sum_{\lambda,\epsilon} |M'_{\mu}|^2$  is used for results with green line. Logarithmic scale is used, but for the ratio (black line) linear scale is used instead. Fraction of presented events (i.e. with photons above 50 MeV) is respectively  $4.2279 \pm 0.0021$  % and  $4.2271 \pm 0.0021$ % of the total samples for the two programs.



(a) cosine of the photon angle with respect to beam is shown. (b) cosine of the  $\pi^+$  angle with respect to the same charge beam is shown.

complete kinematics of  $\gamma^* \rightarrow \pi^+\pi^-\gamma$  process.

Any further investigation of the analogy, would require amplitudes of higher orders. Such an effort can not be justified for scalar QED. From low energy point of view, terms like (12) or (14), should be understood as genuine scalar QED process, and not part of real photon bremsstrahlung. Scalar QED is not supposed to be valid in the regions of phase space where the terms contribute significantly. It is of phenomenological interest to check this limit of scalar QED predictions by direct comparisons with the data. Thanks to present work, higher order genuine bremsstrahlung effects for  $\gamma^* \rightarrow \pi^+\pi^-\gamma$  can be simulated with the help of PHOTOS and one can concentrate on comparison with the data on non-bremsstrahlung parts (12) or (14).

In this paper we have not discussed interference with the photons originating from incoming beams, nor the interference between two consecutive emissions from the same charged line. The first effect, to be solved, require simultaneous treatment of initial state bremsstrahlung and the final one. This is out of scope of work on PHOTOS alone. On the other hand, spin amplitudes are ready for such work. For discussion of interference of two emissions from the same charged line second order matrix element is needed. Fortunately the structure of spin amplitudes for  $\gamma^* \rightarrow \pi^+\pi^-\gamma$  and  $W \rightarrow l\nu$  match this of  $Z \rightarrow l^+l^-\gamma$  [33]. We may expect that the results of that paper and choice of algorithm for matching consecutive emissions, hold for our processes.

We were not discussing virtual corrections. We assume that the dominant part can be included in a factor multiplying Born amplitude and total correction to the total rate is free of any big logarithm. We leave this point for the future work.

Finally, present paper provides numerical tests of PHOTOS Monte Carlo and its construction for the decays where Born level cross section has zero. This is of practical interest for the

program users and also necessary step before an attempt to extension into QCD can be made. Further studies of that type are necessary. To identify building blocks calculations from scalar QED and QED are useful.

## A Matrix element for W decay

The matrix element of the process  $W^-(Q, \lambda) \rightarrow l(p_l, \lambda_l) \bar{\nu}(p_\nu, \lambda_\nu) \gamma(k, \sigma)$  has the form

$$\begin{aligned}
M_{\lambda, \lambda_\nu, \lambda_l}^\sigma(k, Q, p_\nu, p_l) &= \left[ \frac{Q_l}{2k \cdot p_l} b_\sigma(k, p_l) - \frac{Q_W}{2k \cdot Q} (b_\sigma(k, p_l) + b_\sigma(k, p_\nu)) \right] B_{\lambda_l, \lambda_\nu}^\lambda(p_l, Q, p_\nu) \\
&+ \frac{Q_l}{2k \cdot p_l} \sum_{\rho=\pm} U_{\lambda_l, \rho}^\sigma(p_l, m_l, k, 0, k, 0) B_{\rho, -\lambda_\nu}^\lambda(k, Q, p_\nu) \\
&- \frac{Q_W}{2k \cdot Q} \sum_{\rho=\pm} \left( B_{\lambda_l, -\rho}^\lambda(p_l, Q, k) U_{-\rho, -\lambda_\nu}^\sigma(k, 0, k, 0, p_\nu, 0) \right. \\
&\quad \left. + U_{\lambda_l, \rho}^\sigma(p_l, m_l, k, 0, k, 0) B_{\rho, -\lambda_\nu}^\lambda(k, Q, p_\nu) \right), \tag{32}
\end{aligned}$$

where we have introduced the following notation :

$$\begin{aligned}
B_{\lambda_1, \lambda_2}^\lambda(p_1, Q, p_2) &\equiv \frac{g}{2\sqrt{2}} \bar{u}(p_1, \lambda_1) \hat{\epsilon}_W^\lambda(Q) (1 + \gamma_5) v(p_2, \lambda_2), \\
U_{\lambda_1, \lambda_2}^\sigma(p_1, m_1, k, 0, p_2, m_2) &\equiv \bar{u}(p_1, \lambda_1) \hat{\epsilon}_\gamma^\sigma(k) u(p_2, \lambda_2), \\
\delta_{\lambda_1 \lambda_2} b_\sigma(k, p) &\equiv U_{\lambda_1, \lambda_2}^\sigma(p, m, k, 0, p, m), \tag{33}
\end{aligned}$$

$Q_l$  and  $Q_W$  are the electric charges of the fermion  $l$  and the  $W$  boson, respectively, in units of the positron charge,  $\epsilon_\gamma^\sigma(k)$  and  $\epsilon_W^\lambda(Q)$  denote respectively the polarization vectors of the photon and the  $W$  boson. An expression of the function  $U_{\lambda_1, \lambda_2}^\sigma$  in terms of the massless spinors and other notations can be found in [54]. It is easy to check that the three components of the sum contributing to (32) are individually gauge invariant. Note, that the first one coincide with the amplitude at the eikonal approximation.

## References

- [1] R. Kleiss, ed., *oai:cds.cern.ch:367653. Workshop on Z Physics at LEP1 : General Meetings, v.3 : Z physics at LEP 1 - Event generators and software*. Coordinated and supervised by R. Kleiss.
- [2] S. Jadach, G. Passarino, and R. Pittau, eds., *Reports of the working groups on precision calculation for LEP-2 physics. Proceedings, Monte Carlo Workshop, Geneva, Switzerland, 1999-2000*.
- [3] M. Kobayashi, Nobel Prize Lecture: CP Violation and Flavor Mixing.
- [4] Belle Collaboration, K. Abe *et al.*, *Phys. Rev. Lett.* **98** (2007) 181804, hep-ex/0608049.
- [5] BABAR Collaboration, B. Aubert *et al.*, *Phys. Rev.* **D67** (2003) 032002, hep-ex/0207097.
- [6] F. A. Berends, R. Kleiss, and S. Jadach, *Comput. Phys. Commun.* **29** (1983) 185–200.
- [7] S. Jadach, B. F. L. Ward, and Z. Was, *Comput. Phys. Commun.* **66** (1991) 276–292.
- [8] T. Sjostrand, *Comput. Phys. Commun.* **82** (1994) 74–90.
- [9] G. Corcella *et al.*, *JHEP* **01** (2001) 010, hep-ph/0011363.
- [10] D. R. Yennie, S. C. Frautschi, and H. Suura, *Ann. Phys.* **13** (1961) 379–452.
- [11] S. Jadach, MPI-PAE/PTh 6/87.
- [12] S. Jadach, B. F. L. Ward, and Z. Was, *Phys. Rev.* **D63** (2001) 113009, hep-ph/0006359.
- [13] E. A. Kuraev, L. N. Lipatov, and V. S. Fadin, *Sov. Phys. JETP* **44** (1976) 443–450.
- [14] E. A. Kuraev, L. N. Lipatov, and V. S. Fadin, *Sov. Phys. JETP* **45** (1977) 199–204.
- [15] I. I. Balitsky and L. N. Lipatov, *Sov. J. Nucl. Phys.* **28** (1978) 822–829.
- [16] V. S. Fadin and L. N. Lipatov, *Phys. Lett.* **B429** (1998) 127–134, hep-ph/9802290.
- [17] B. I. Ermolaev, M. Greco, and S. I. Troyan, *Acta Phys. Polon.* **B38** (2007) 2243–2260, 0704.0341.
- [18] V. G. Gorshkov, V. N. Gribov, L. N. Lipatov, and G. V. Frolov, *Sov. J. Nucl. Phys.* **6** (1968) 262.
- [19] V. G. Gorshkov, V. N. Gribov, L. N. Lipatov, and G. V. Frolov, *Sov. J. Nucl. Phys.* **6** (1968) 95.
- [20] L. V. Gribov, E. M. Levin, and M. G. Ryskin, *Phys. Rept.* **100** (1983) 1–150.

- [21] B. R. Webber, *Ann. Rev. Nucl. Part. Sci.* **36** (1986) 253–286.
- [22] B. I. Ermolaev, M. Greco, and S. I. Troyan, *Phys. Lett.* **B522** (2001) 57–66, hep-ph/0104082.
- [23] B. I. Ermolaev and S. I. Troyan, *Phys. Lett.* **B666** (2008) 256–261, 0805.2278.
- [24] CDF Collaboration, A. A. Affolder *et al.*, *Phys. Rev.* **D65** (2002) 092002.
- [25] M. Derrick and T. Gottschalk, Contributed to Summer Study on the Design and Utilization of the Superconducting Super Collider, Snowmass, Colo., Jun 23-Jul 13, 1984.
- [26] L. Berny, *Z. Phys.* **C48** (1990) 227–229.
- [27] A. van Hameren and Z. Was, *Eur. Phys. J.* **C61** (2009) 33–49, 0802.2182.
- [28] E. Barberio, B. van Eijk, and Z. Was, *Comput. Phys. Commun.* **66** (1991) 115–128.
- [29] E. Barberio and Z. Was, *Comput. Phys. Commun.* **79** (1994) 291–308.
- [30] F. A. Berends, R. Kleiss, and S. Jadach, *Nucl. Phys.* **B202** (1982) 63.
- [31] E. Richter-Was and Z. Was, CPT-87/P-2080.
- [32] S. Jadach, B. F. L. Ward, and Z. Was, *Comput. Phys. Commun.* **130** (2000) 260–325, hep-ph/9912214.
- [33] Z. Was, *Eur. Phys. J.* **C44** (2005) 489–503, hep-ph/0406045.
- [34] E. Richter-Was, *Z. Phys.* **C64** (1994) 227–240.
- [35] E. Richter-Was, *Z. Phys.* **C61** (1994) 323–340.
- [36] P. Golonka and Z. Was, *Eur. Phys. J.* **C45** (2006) 97–107, hep-ph/0506026.
- [37] P. Golonka and Z. Was, *Eur. Phys. J.* **C50** (2007) 53–62, hep-ph/0604232.
- [38] G. Nanava and Z. Was, *Eur. Phys. J.* **C51** (2007) 569–583, hep-ph/0607019.
- [39] K. Hamilton and P. Richardson, *JHEP* **07** (2006) 010, hep-ph/0603034.
- [40] P. Golonka, T. Pierzchala, and Z. Was, *Comput. Phys. Commun.* **157** (2004) 39–62, hep-ph/0210252.
- [41] N. Davidson, P. Golonka, T. Przedzinski, and Z. Was, 0812.3215.
- [42] V. N. Gribov and L. N. Lipatov, *Sov. J. Nucl. Phys.* **15** (1972) 438–450.
- [43] J. C. Collins, D. E. Soper, and G. Sterman, *Nucl. Phys.* **B261** (1985) 104.

- [44] W. Furmanski, Lectures on QCD given to the students of Jagellonian University, see also [?].
- [45] A. Andonov, S. Jadach, G. Nanava, and Z. Was, *Acta Phys. Polon.* **B34** (2003) 2665–2672, hep-ph/0212209.
- [46] G. Nanava and Z. Was, *Acta Phys. Polon.* **B34** (2003) 4561–4570, hep-ph/0303260.
- [47] G. Rodrigo, H. Czyz, J. H. Kuhn, and M. Szopa, *Eur. Phys. J.* **C24** (2002) 71–82, hep-ph/0112184.
- [48] F. A. Berends, R. Kleiss, J. P. Revol, and J. P. Vialle, *Z. Phys.* **C27** (1985) 155.
- [49] D. Bardin, S. Jadach, T. Riemann, and Z. Was, *Eur. Phys. J.* **C24** (2002) 373–383, hep-ph/0110371.
- [50] T. Kinoshita, *J. Math. Phys.* **3** (1962) 650.
- [51] T. D. Lee and M. Nauenberg, *Phys. Rev.* **B133** (1964) 1549.
- [52] H. Czyz, A. Grzelinska, J. H. Kuhn, and G. Rodrigo, *Eur. Phys. J.* **C27** (2003) 563–575, hep-ph/0212225.
- [53] S. Jadach, E. Richter-Was, B. F. L. Ward, and Z. Was, *Phys. Lett.* **B253** (1991) 469–477.
- [54] S. Jadach, B. F. L. Ward, and Z. Was, *Phys. Lett.* **B449** (1999) 97–108, hep-ph/9905453.
- [55] A. Andonov *et al.*, *Comput. Phys. Commun.* **174** (2006) 481–517, hep-ph/0411186.